Transactions of the Materials Research Society of Japan, **29** (8) (2004)

Nucleation Mechanism of Boride Nanoparticles in Induction Thermal Plasmas

Takayuki Watanabe Tsuyoshi Ibe, Yoshiyuki Abe*, Yoshiro Ishii* and Kenji Adachi*
Research Laboratory for Nuclear Reactors, Tokyo Institute of Technology, Tokyo 152-8550, Japan
Fax: 81-3-5734-3058, e-mail: watanabe@nr.titech.ac.jp
*Central Research Laboratory, Sumitomo Metal Mining Co., Ltd., Chiba 272-8588, Japan

Induction thermal plasmas were used for production of rare-earth boride nanoparticles. Rare-earth boride is attractive materials because of their high melting temperature, high electrical conductivity and low work function. Another purpose is to investigate the condensation mechanism of vapor mixture of rare-earth metal and boron in thermal plasmas. Investigation of physical and chemical processes in thermal plasma processing is indispensable for production of nanoparticles. Premixed feed powders of rare-earth oxide, boron and carbon were injected into the thermal plasma. In the thermal plasma, the feed powders were evaporated and reacted with boron. After the evaporation and reaction, the vapor was rapidly cooled after the plasma flame. Boron, lanthanum and cerium have wide liquid range between the nucleation and melting temperatures, resulting in better preparation of boride. Induction thermal plasmas provide a powerful tool for the preparation of rare-earth boride nanoparticles because the composition in nanoparticles can be well controlled.
Key words: Induction thermal plasma, Nanoparticle, LaB_6, CeB_6, Nucleation mechanism

1. INTRODUCTION

Induction thermal plasmas have been used for production of high-quality and high-performance materials, such as nanoparticles synthesis, thin film deposition, plasma spraying and powder treatments. These attractive material processes result from distinctive advantages; these advantages include high enthalpy to enhance reaction kinetics, high chemical reactivity, large volume with low velocity, oxidation and reduction atmospheres in accordance with required chemical reactions, and rapid quenching to produce chemical non-equilibrium materials. These advantages increase the advances and demands in plasma chemistry and plasma processing, such as preparation of various kinds of nanoparticles in metallic and ceramic systems.

The purpose of this paper is to prepare rare-earth boride nanoparticles by induction thermal plasmas. Rare-earth boride is attractive materials because of their high melting temperature, high electrical conductivity and low work function. Therefore these nanoparticles would be applied for electromagnetic shielding, and solar control windows with interaction with IR or UV light. Some reports about the preparation of boride nanoparticles were published previously; YB_{66} nanoparticles were prepared by plasma chemical process using starting powders of YB_4 and boron [1]. TiB_2 nanoparticles were synthesized in the vapor-phase reaction of sodium with $TiCl_4$ and BCl_3 [2].

Another purpose is to investigate the condensation mechanism of vapor mixture of rare-earth metal and boron in thermal plasmas. Investigation of physical and chemical processes in thermal plasma processing is indispensable for nanoparticles production. Co-condensation process of metal vapors was investigated for Nb-Al and Nb-Si systems [3], Nb-Si and V-Si

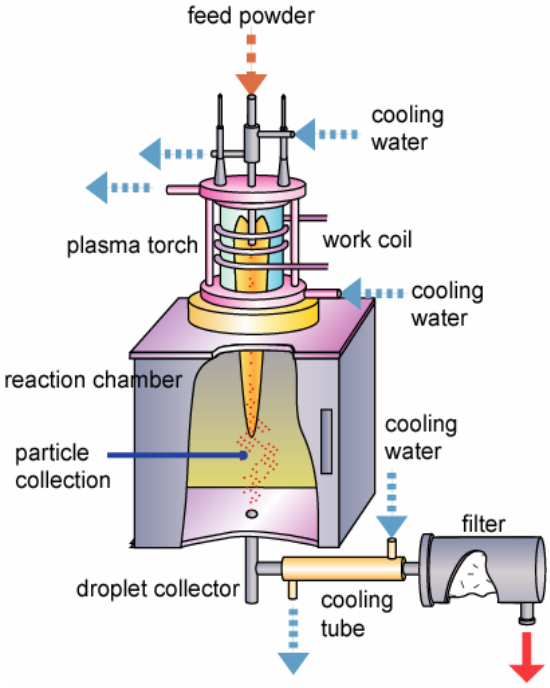

Fig. 1 Experimental set-up for nanoparticle preparation.

systems [4]. Recently, formation mechanism was investigated for silicide nanoparticles [5] and for boride/nitride mixture [6]. Vaporization process for Ti-Si, V-Si and Mo-Si systems were also investigated [7]. For nanoparticle preparation with stoichiometric composition, the vaporization and condensation rates of the constituent materials should be controlled in the case of large difference in the vapor pressure.

2. EXPERIMENTAL SET-UP

Figure 1 shows a schematic illustration of experimental set-up for nanoparticle production with induction thermal plasmas. The set-up consists of a plasma torch, a reaction chamber, and a power supply (4 MHz). Total system was operated at 25 kW under atmospheric pressure of argon. Premixed powders of La_2O_3, boron and carbon were injected into the plasma at the feed rate of 0.1 g/min. Premixed powders of CeO_2, boron and carbon were also used for the preparation of CeB_6. The feed powders used in this study are La_2O_3 (average: 14.4 μm), CeO_2 (average: 20.2 μm), boron (average: 15.0 μm), and carbon (average: 1.34 μm). The feeding rate and the carbon content in the feed powders were changed in the experiments.

In the thermal plasma, the feed powders were evaporated and reacted with boron. After the evaporation and reaction, the vapor was rapidly cooled after the plasma flame. Through the cooling process, boride nanoparticles were prepared. The prepared nanoparticles were collected at quenching condition by the water-cooled coil.

The structures of the prepared nanoparticles were determined by x-ray diffractometry (XRD, Mac Science MXP3TA). Concentrations of lanthanum and boron in the prepared particles were determined by inductively coupled plasma spectrometry (ICP, Seiko Instruments SPS4000), while that of carbon were measured by carbon determinator (LECO EC12). The size distribution of the particles was measured from the photographs of transmission electron microscopy (TEM) for about 1000 particles. TEM observations as well as electron diffractometry (ED) were performed on JEOL JEM-2010 operated at an accelerating voltage of 200 kV.

3. EXPERIMENTAL RESULTS

3.1 La-B-C systems

The XRD spectrum charts of the prepared nanoparticles for La_2O_3-B-C system with Ar plasmas are demonstrated in Fig. 2. LaB_6 and La_2O_3 were identified from the XRD spectrum peak of the as-prepared particles. After separation of the as-prepared particles by ultrasonic dispersion, the nanoparticles were collected in the suspension, and the agglomerated particles were collected in the precipitate.

TEM photograph of the prepared nanoparticles for La_2O_3-B-C system was shown in Fig. 3. The particle size distribution shown in Fig. 4

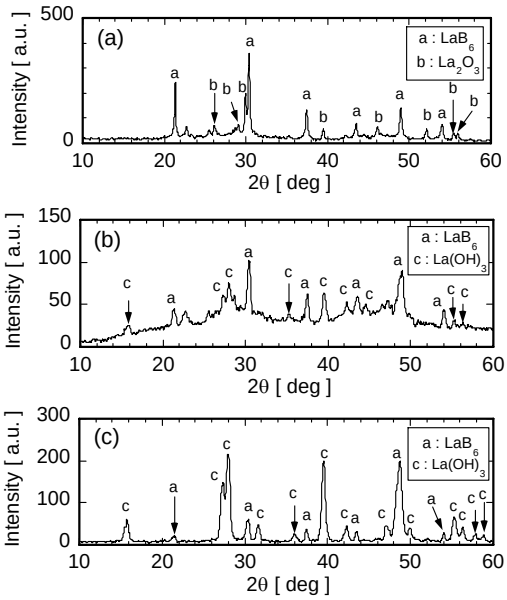

Fig. 2 XRD charts of nanoparticles: La_2O_3:B:C =1:12:3; (a) as-prepared particles, (b) nanoparticles in suspension, (c) agglomerated particles in precipitation.

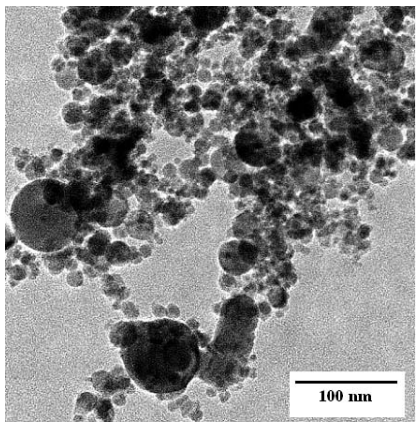

Fig. 3 TEM photograph of nanoparticles; La_2O_3:B:C = 1:12:3.

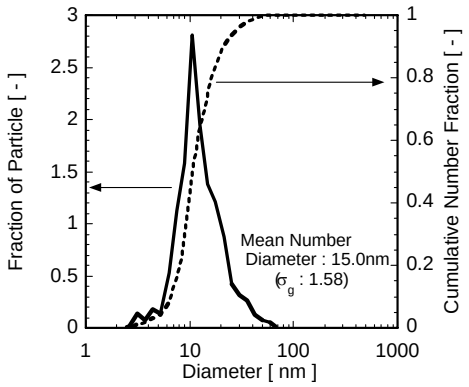

Fig. 4 Particle size distribution of nanoparticles: La_2O_3:B:C = 1:12:3.

evaluated from the TEM photographs presents the average particles size of 15.0 nm with the geometrical standard distribution of 1.58. Nanoparticles are mainly composed of LaB_6 with small fraction of $La(OH)_3$ made from hydration of La_2O_3 particles at ultrasonic dispersion. The agglomerated particles are identified as LaB_6, $La(OH)_3$, $LaBO_3$ with unreacted boron from XRD and ED analysis as shown in Figs. 2(c) and 5.

Figure 6 shows the effect of carbon mass fraction in the feed powders on the nanoparticle composition. The prepared amount of LaB_6 increases with the carbon content, because the injected La_2O_3 is easily reduced by carbon during the plasma process. Increasing in the carbon content in the feed powders also causes the increase in the carbon content in the prepared particles. However the carbon in the prepared particles can be separated by hydrochloric acid treatment (3 N) during 20 min at room temperature. The production yield was 40 % in these experiments. Therefore, induction thermal plasmas provide a new preparation method for boride nanoparticles.

3.2 Ce-B-C systems

The prepared nanoparticles for CeO_2-B-C system with Ar plasmas include CeB_6 and Ce_2O_3. After separation of the as-prepared particles by ultrasonic dispersion, the nanoparticles were collected in the suspension, and the agglomerated particles were collected in the precipitate. Nanoparticles are mainly composed of CeB_6 with small fraction of CeO_2 made from oxidation of Ce_2O_3 at drying after ultrasonic dispersion.

Figure 7 shows the comparison of nanoparticle composition for La_2O_3-B-C and CeO_2-B-C systems. The ratio of LaB_6 to La_2O_3 is larger than the ratio of CeB_6 to Ce_2O_3 in the as-prepared particles. The better preparation of LaB_6 than that of CeB_6 is attributed to lower ΔG of lanthanum boridation than that of cerium boridation as shown in Fig. 8.

4. DISCUSSIONS

Homogeneous nucleation rate has been proposed by Girshick et al. [8]. They derived the expression as an extension of kinetic nucleation theory. The proposed expression can be used over a wide range of physical conditions. Furthermore, the expression for homogenous nucleation, J, was consistent with experimental data. Therefore Eq. (1) was used for the estimation of critical saturation ratio.

$$J = \frac{\beta_{11} n_s S}{12} \sqrt{\frac{\Theta}{2\pi}} \exp\left[\Theta - \frac{4\Theta^3}{27(\ln S)^2}\right] \qquad (1)$$

where n_s is the equilibrium saturation monomer concentration at temperature T, β_{11} the collision frequency function between monomers, and S the saturation ratio. The dimensionless surface tension Θ is given by

$$\Theta = \sigma s_1 / kT \qquad (2)$$

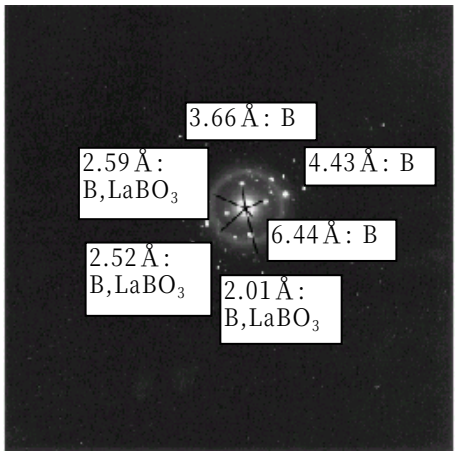

Fig. 5 ED analysis of agglomerated particles: La_2O_3:B:C = 1:12:3.

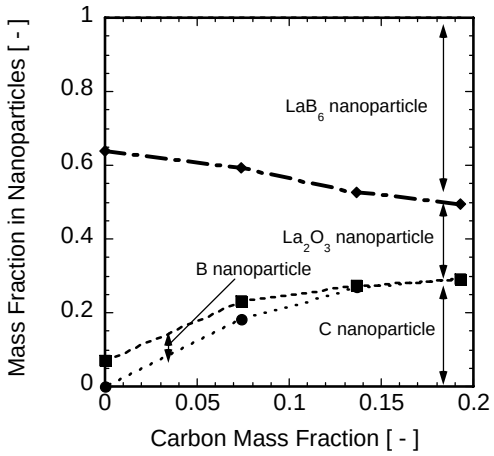

Fig. 6 Effect of carbon mass fraction in feed powders on nanoparticle composition.

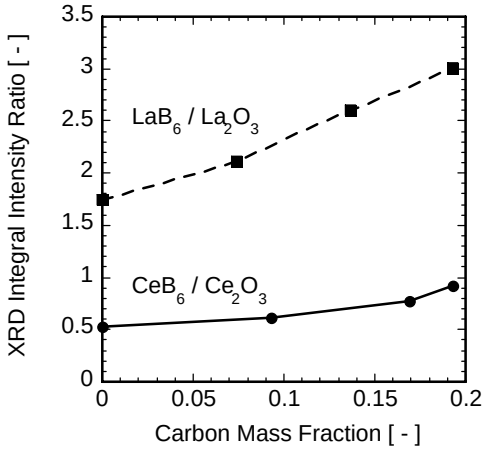

Fig. 7 Comparison of nanoparticle composition for La_2O_3-B-C and CeO_2-B-C systems.

where σ is the surface tension, and s_1 the monomer surface area. The collision frequency function β_{ij} can be estimated by Eq. (3) when the Knudsen number is more than 10 [9].

$$\beta_{ij} = \left(\frac{3v_1}{4\pi}\right)^{1/6} \sqrt{\frac{6kT}{\rho_p}\left(\frac{1}{i}+\frac{1}{j}\right)} \times \left(i^{1/3}+j^{1/3}\right)^2 \quad (3)$$

where ρ_p is the particle mass density and v_1 the monomer volume. In this model, the particle nucleation is due to the monomer collision, therefore $i = j = 1$.

Relationship between the nucleation rate and saturation ratio is shown in Fig. 9. The nucleation rate is strongly dependent on the surface tension and saturation ratio. When the nucleation rate is over 1.0 cm^{-3} s^{-1}, particle formation can be conveniently observed experimentally. Therefore the corresponding value of saturation ratio is defined as the critical saturation ratio [9]. The critical saturation ratio of boron was estimated to be 2, while lanthanum and cerium have the critical saturation ratio of 14 and 16, respectively. Carbon has the highest critical saturation ratio of 42.

The nucleation temperature at the critical saturation ratio is presented in Fig. 10 for the injected powder materials. The nucleation temperature of carbon corresponds to the melting temperature, while boron, lanthanum and cerium have wide liquid range between the nucleation and melting temperatures. The wide liquid range combination of boron with rare-earth metals leads to better preparation of rare-earth boride nanoparticles.

5. CONCLUSION

Boron, lanthanum and cerium have wide liquid range between the nucleation and melting temperatures, resulting in better preparation of LaB_6 and CeB_6 nanoparticles. Induction thermal plasmas provide a powerful tool for the preparation of functional nanoparticles because the phase and composition in nanoparticles can be well controlled.

REFERENCES

[1] J. Y. Huang, T. Ishigaki, T. Tanaka, S. Horiuchi, *J. Mater. Sci.*, **33**, 4141 (1998).
[2] R. L. Axelbaum, D. P. Dufaux, and C. A. Frey, *J. Mater. Res.*, **11**, 948 (1996).
[3] T. Harada, T. Yoshida, T. Kozeki and K. Akashi, *J. Japan Inst. Metals*, **45**, 1138 (1981).
[4] Y. Anekawa, T. Koseki, T. Yoshida and K. Akashi, *J. Japan Inst. Metals*, **49**, 451 (1985).
[5] T. Watanabe, A. Nezu, Y. Abe and Y. Ishii, *Thin Solid Films*, **435**, 27 (2003).
[6] K. Katsuda, T. Watanabe, Y. Abe and Y. Ishii, *Trans. Mater. Res. Soc. Japan*, **27**, 137 (2002).
[7] T. Watanabe, H. Itoh and Y. Ishii, *Thin Solid Films*, **390**, 44 (2001).
[8] S. L. Girshick, C. P. Chiu and P. H. McMurry, *Aerosol Sci. Tech.*, **13**, 465 (1990).
[9] S. K. Friedlander, Smoke, Dust and Haze, John Wiley and Sons (1977).

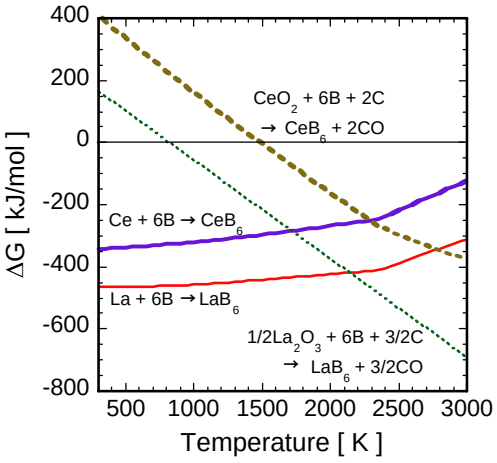

Fig. 8 Comparison of gibbs free energy between La boridation and Ce boridation.

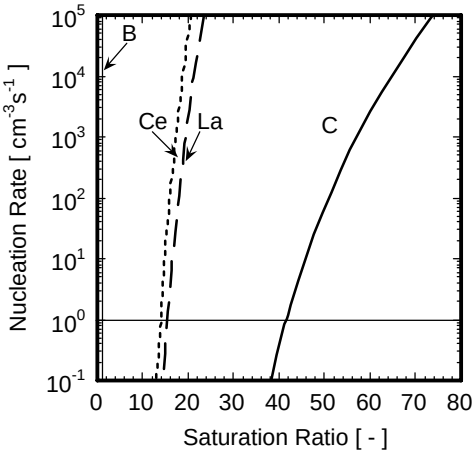

Fig. 9 Relationship between homogenous nucleation rate and saturation ratio for La, Ce, B and C.

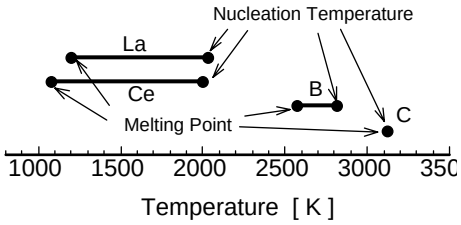

Fig. 10 Nucleation and melting temperature of La, Ce, B and C.